OPEN ACCESS
Journal of Innovative Optical Health Sciences
Vol. 16, No. 4 (2023) 2243004 (8 pages)

DOI: 10.1142/S1793545822430040

World Scientific
www.worldscientific.com

Deep-skin third-harmonic generation (THG) imaging *in vivo* excited at the 2200 nm window

Xinlin Chen, Yi Pan, Ping Qiu* and Ke Wang†
Key Laboratory of Optoelectronic Devices and Systems of Ministry of Education and Guangdong Province
College of Physics and Optoelectronic Engineering
Shenzhen University, Shenzhen 518060, P. R. China
**pingqiu@szu.edu.cn*
†*kewangfs@szu.edu.cn*

Received 11 July 2022
Accepted 14 September 2022
Published 27 October 2022

The skin is heterogeneous and exerts strong scattering and aberration onto excitation light in multiphoton microscopy (MPM). Shifting to longer excitation wavelengths may help reduce skin scattering and aberration, potentially enabling larger imaging depths. However, previous demonstrations of skin MPM employ excitation wavelengths only up to the 1700 nm window, leaving an open question as to whether longer excitation wavelengths are suitable for deep-skin MPM. Here, in order to explore the longer-wavelength territory, first, we demonstrate characterization of the broadband transmittance of excised mouse skin, revealing a high transmittance window at 2200 nm. Then, we demonstrate third-harmonic generation (THG) imaging in mouse skin *in vivo* excited at this window. With 9 mW optical power on the skin surface operating at 1 MHz repetition rate, we can get THG signals of 250 μm below the skin surface. Comparative THG imaging excited at the 1700 nm window shows that as imaging depth increases, THG signals decay even faster than those excited at 2200 nm. Our results thus uncover the 2200 nm window as a new, promising excitation window potential for deep-skin MPM.

Keywords: Third-harmonic generation; 2200 nm; 1700 nm; skin.

1. Introduction

The skin is the largest organ and the first defense barrier of the body with the main functions of protection, regulation, and sensation. In order to visualize and investigate skin structures and their functions with cellular resolution, optical imaging is an indispensable technology. Among the various optical imaging modalities, multiphoton microscopy (MPM) has its unique niche due to its three-dimensional (3D) sectioning, lower tissue scattering due to long excitation wavelength, and intrinsic multiphoton signal generation mechanism, including second/third harmonic and endogenous multiphoton fluorescence.[1–3] As a result, MPM can acquire the structures and capture the dynamics of

skin *in vivo*, in animal models and even on human subjects.[4–7]

Skin is a multilayered structure and thus highly heterogenous. Tissue heterogeneity is known to impose dramatic scattering and aberration onto the excitation light,[8,9] which degrades MPM signal levels and resolution as imaging depth increases. A potential solution to reducing tissue scattering and aberration is shifting to longer excitation wavelengths.[10–12] When choosing an excitation wavelength for MPM, tissue absorption is another factor that needs consideration. For most biological tissues, the major component is water. So excitation wavelengths typically lie within low water absorption windows. So far, three excitation windows have been demonstrated as suitable for skin MPM— the 800, 1300 and 1700 nm window. Among them, the 1700 nm window is especially suitable for deep-skin MPM.[13–15] However, it remains unknown whether there is a longer excitation window suitable for deep-skin MPM.

2. Materials and Methods

2.1. *Experimental setup*

Through both water absorption and tissue transmittance measurements, it has been shown that water absorption reaches a local minimum, and biological tissue transmittance reaches a local maximum at the 2200 nm window (roughly 2060–2400 nm).[16–18] These measurements imply that the 2200 nm window is a potential excitation window for deep-skin MPM.

A spectrometer (Lambda 900, Perkin Elmer) was used to measure the broadband transmittance of the freshly excised mouse skin, spanning from 500 nm to 2500 nm. A pinhole with a diameter of ~ 2 mm was placed in front of the skin to sample a relatively uniform area. The whole spectrum was acquired with a 2 nm step in wavelength.

However, due to the lack of proper instrumentation at this window, skin MPM has never been demonstrated. Recently, we have developed a fiber-based 2200 nm femtosecond laser and the corresponding laser scanning microscope.[19] It is our aim in this paper to explore skin MPM in this long excitation window, focusing on imaging depth, signal level, spatial resolution, and its comparison with the 1700 nm window.

The experimental setup is shown in Fig. 1(a) and similar to Ref. 19. Both 2200 nm and 1700 nm femtosecond pulses were generated through the nonlinear optical effect of soliton self-frequency shift (SSFS)[20,21] pumped by a 1550 nm, 1 MHz, 500 fs fiber laser (FLCPA-02CSZU, Calmar), but in different optical waveguides. 2200 nm pulses were

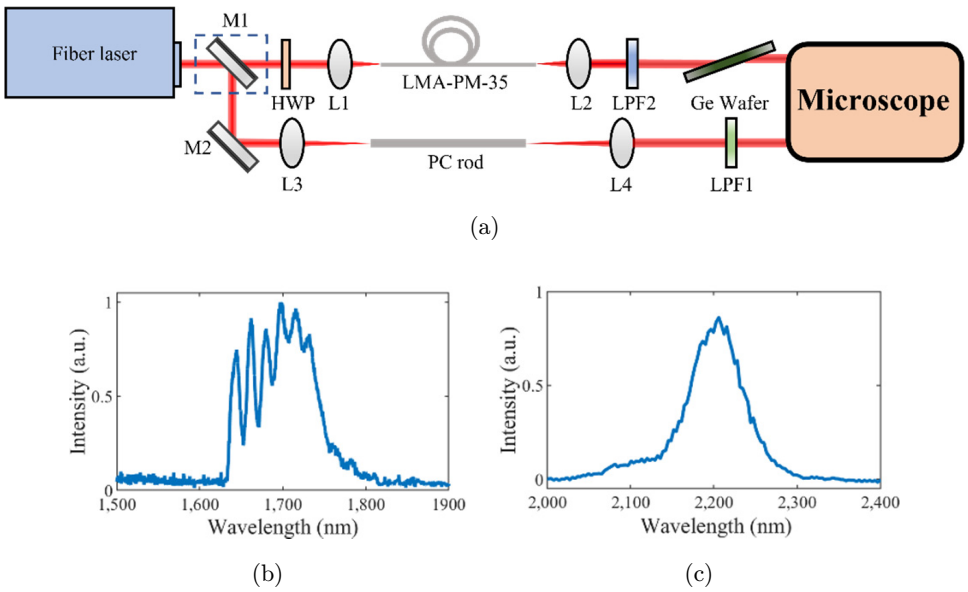

Fig. 1. Experimental setup (a). L1: $f = 50$ mm lens; L2: $f = 40$ mm lens; L3: $f = 100$ mm lens; L4: $f = 75$ mm lens; LPF1: 2055 nm long-pass filter; LPF2: 1635 nm long-pass filter; HWP: half-wave plate; M1, M2: silver-coated mirror, M1 is removable to switch the path between 2200 nm and 1700 nm; LMA: 65-cm large-mode-area fiber, PC rod: 44-cm photonic-crystal rod. (b) Measured 1700 nm soliton spectrum. (c) Measured 2200 nm soliton spectrum.

generated in a 65 cm largemode-area (LMA-PM-35, NKT Photonics) fiber. The optical spectrum measured after a 2055 nm long-pass filter (LP-2055 nm, Spectrogon) was shown in Fig. 1(c). A 2 mm germanium wafer placed at Brewster angle compressed the pulse width on the sample to 98 fs.[19] Pumped by the same fiber laser, the 1700 nm soliton pulses were generated in a 44 cm photonic-crystal rod (SC-1500/100-Si-ROD, NKT Photonics), with a measured spectrum shown in Fig. 1(b) filtered by a 1635 nm long-pass filter (1635LPF, Omega Optical). The pulse width on the sample was 88 fs.

The optics in the laser scanning microscope (MOM, Sutter) was optimized for the 2200 nm window. Both the scan lens (LA5763-D, Thorlabs) and the tube lens (ACA254-200-D, Thorlabs) have high transmittance at the 2200 nm window. Among the various immersion objective lenses, a numerical aperture (NA) = 1.05 water-immersion objective lens (XLPLN25XWMP2-SP1700, working distance = 2 mm, Olympus) was chosen based on its measured transmittance.[22] The objective lens was underfilled to avoid extra loss of power on the sample (the effective NA is 0.53 for both excitations). D_2O immersion was used instead of H_2O immersion, due to its lower absorption coefficient at the 2200 nm window 16. Third-harmonic generation (THG) signals were epi-detected by the same GaAs PMT (H7422p-50, Hamamatsu) for both excitations, but with different bandpass filters: for 2200 nm THG, a 732/68 nm bandpass filter (FF01-732/68-25, Semrock) was used, while for 1700 nm THG, a 560/94 nm bandpass filter (FF01-560/94-25, Semrock) was used.

The maximum optical power of the 2200 nm excitation on the sample was 9 mW with both optics and immersion medium considered. For skin imaging, the acquisition speed was 2 ms/line with 2 averages, with a resultant frame rate of 0.5 frame/s for a pixel size of 512 × 512.

2.2. *Animal procedures*

Animal procedures were reviewed and approved by Shenzhen University. Measurements and imaging were carried out on Balb/C mice (12–14 weeks old, Guangdong Medical Laboratory Animal Center). For *in vivo* imaging, mice were anesthetized with isoflurane using a gaseous anesthesia system (Matrx VIP 3000, Midmark). Body temperature was kept at ∼ 37°C with a heating pad. The dorsal skin was depilated and rinsed with phosphate-buffered saline before imaging. The skin was fixed by a homemade titanium metal piece with a cover glass glued by dental cement to seal the skin window for imaging.

For *ex vivo* measurement, skin samples were excised from the dorsal area of mice, which is the same as that in imaging *in vivo*. We removed the skin above the superficial fascia with a scalpel after depilation. The excised skin sample was approximately 15 × 10 mm^2, with a thickness of ∼ 400 μm. Saline was added onto the sample when sealed between a cover glass and a glass slide to keep the skin moisturized. Transmittance measurement was performed immediately after sample preparation.

3. Results

3.1. *Ex vivo transmittance measurement*

First, we measured the broadband transmittance of the freshly excised mouse skin. From the results we can clearly identify three windows with relatively high transmittance: 1300, 1700 and 2200 nm windows (Fig. 2). For 1300, 1700 and 2200 nm excitations, the measured transmittances are 3.18%, 3.18% and 2.48%, while the water absorption coefficients are 1.31, 5.80 and 19.69 cm^{-1}, respectively. These results are in agreement with previous MPM experiments excited at both the 1300 and 1700 nm window. Although below the 1300 nm window the transmittance decreases, we note that so far the most widely adopted excitation for skin MPM lies within the 800 nm window, which can be conveniently excited by mode-locked Ti:Sa lasers. Besides, another key advantage is that excitation at the 800 nm window enables two-photon fluorescence microscopy from endogenous fluorophores.

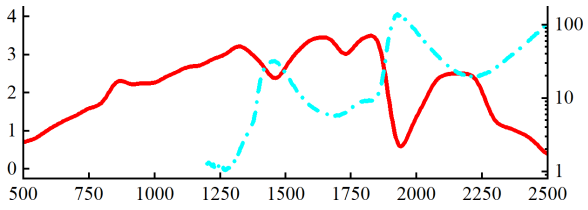

Fig. 2. (Color online) Measured transmittance of the freshly excised mouse skin from 500 nm to 2500 nm (transmittance, left ordinate, red line). Measured water absorption α_A from 1200 nm to 2500 nm[16] (absorption coefficient, right ordinate, blue dash-dotted line).

In order to qualitatively understand the existence of these three excitation windows, we also plotted water absorption spectrum from 1200 nm to 2500 nm (Fig. 2).[16] We can see that the three excitation windows roughly overlap with the local minima in water absorption. Besides, strong water absorption around 1450 and 1925 nm overlap with local minima in skin transmittance. The discrepancy in precise overlapping is due to the following: (1) Transmittance includes the overall contribution from skin absorption and scattering. (2) Skin absorption includes more than water absorption. In spite of this discrepancy, we can still conclude that for efficient transmittance through skin, the excitation wavelength should lie within a relatively low water absorption window. Consequently, the 2200 nm window seems potentially advantageous for deep-skin MPM, judging from this transmittance measurement.

Ex vivo measurement as a useful guidance, cannot be equated with *in vivo* measurement in MPM. So next, we performed THG imaging of the mouse skin *in vivo* excited at both 2200 and 1700 nm. The optical powers for both excitations on the skin surface were increased as imaging depth increased. For fair comparison, from 160 μm below the skin surface to the deepest, we kept the maximum optical power on the sample the same (9 mW) for both 2200 and 1700 nm excitations.

3.2. *Deep-skin THG imaging in vivo at 1700 and 2200 nm window*

Figure 3 shows 3D stacks acquired with excitation at either 1700 nm or 2200 nm. Each image (including those in the 3D stacks) is individually enhanced in contrast with the same maximum pixel brightness. As imaging depth increases, both 1700 and 2200 nm THG imaging results show similar skin structures of stratum corneum (Figs. 3(b) and 3(c)), sebaceous glands (Figs. 3(d) and 3(e)) and adipocytes (Figs. 3(f) and 3(g)). However, the most notable feature is that 2200 nm THG images show deeper penetration into the skin than 1700 nm: From 220 μm to 250 μm below the skin surface, adipocytes in 2200 nm THG images can be clearly resolved. In sharp contrast, at similar imaging depths, they cannot be resolved in 1700 nm THG images. These results show that with the same optical power on the skin surface, 2200 nm excitation enables a larger penetration depth than 1700 nm. The images with enhanced contrast in Fig. 3 cannot be used for direct THG signal comparison. In order to better illustrate the THG signal difference deep in the skin with both excitations, we excerpted THG images from acquired 3D stacks at the same imaging depth without enhancing the contrast. For each pair of images, the same color scale denoting the signal level was used for both excitations (Fig. 4).

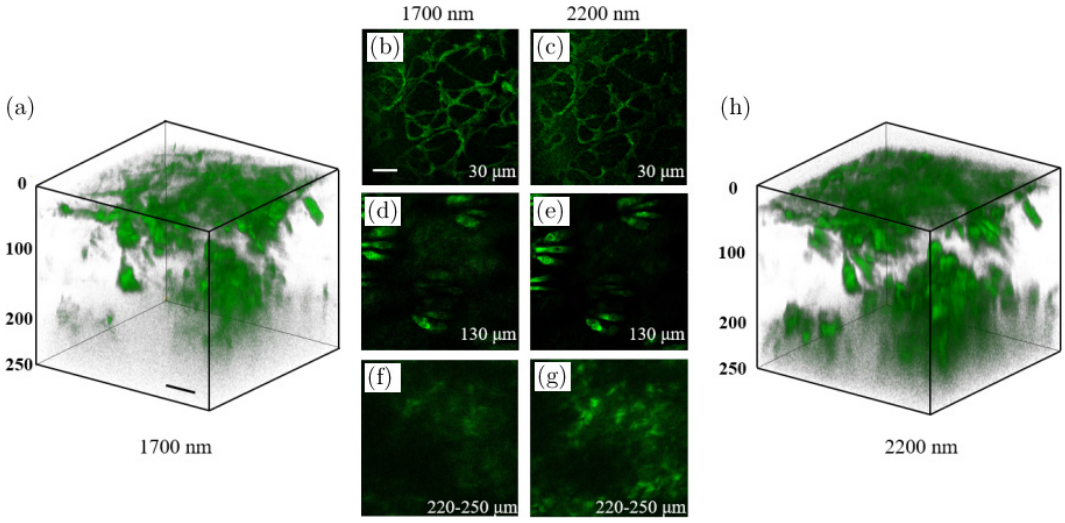

Fig. 3. THG images with 1700 (a), (b), (d), (f) and 2200 nm (c), (e), (g), (h) excitations. (a), (h) 3D-reconstructed stacks. (b)–(g) two-dimensional (2D) images from the stacks. The imaging depths below the skin surface were indicated in each 2D image. Each image is individually enhanced in contrast with a resultant maximum pixel brightness of 65,535. Scale bars: 50 μm; pixel size: 512 × 512.

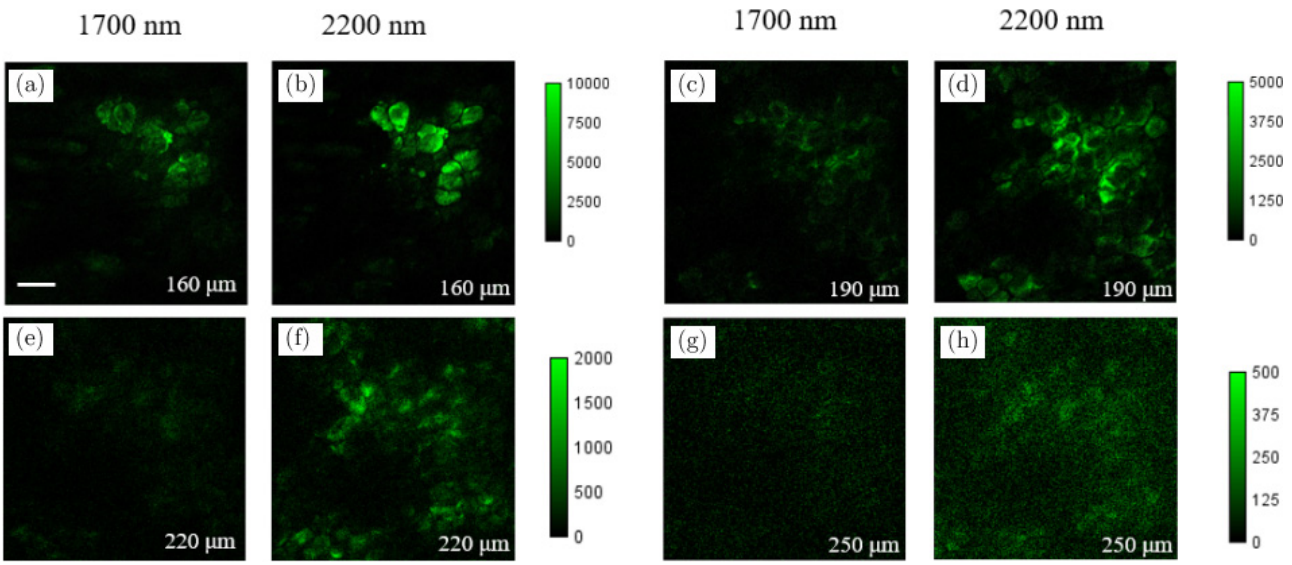

Fig. 4. THG images acquired with 1700 nm (a), (c), (e), (g) and 2200 nm excitation (b), (d), (f), (h), at different imaging depths below the skin surface as indicated in each image. Color scale denoting THG signal is the same for each image pair. Scale bars: 50 μm; pixel size: 512 × 512.

At $z = 160\,\mu$m, both images show similar THG signals. However, as imaging depth increases, THG signals of 1700 nm become lower than 2200 nm THG images at the same depth. To quantitatively compare the THG signal decay with both excitations, we took the following procedure: (1) For images acquired below 160 μm, in which both excitation powers on the sample were 9 mW, we calculated the THG signals S_{2200} and S_{1700} of both excitations for each image. THG signals were calculated as mean values of the image. (2) Then we calculated the ratio S_{2200}/S_{1700}, normalized it at $z = 160\,\mu$m and plotted it as a function of imaging depth z. The resultant ratio is shown in Fig. 5. As expected, the ratio increases with the increasing of z, which is in agreement with the imaging results. Besides, we also calculated the signal-to-background ratio (SBR) for Fig. 4, defined as the mean THG signal ratio between the maximum and minimum 1% pixels. The results summarized in Table 1 show that both THGs acquired at 2200 nm show higher SBRs. We thus conclude that compared with 1700 nm excitation, 2200 nm excitation performs better in deep-skin MPM, and THG decays less as imaging depth increased at that window.

In order to characterize and compare spatial resolutions with both excitations, we imaged structures with the smallest lateral size, in our case the membrane of adipocytes, shown in Figs. 6(a) and 6(c). Then, we plotted line profiles along the adipocyte membrane (Figs. 6(b) and 6(d)). The full-width-at-half-maximum (FWHM) of this line profile is a measure of the spatial resolution. The measured line profiles were fitted with Gaussian

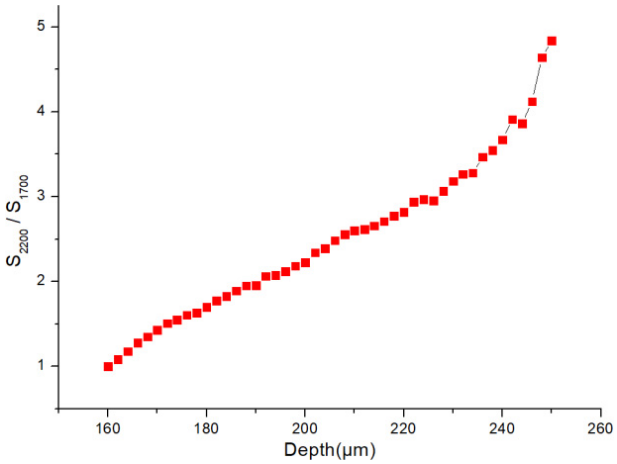

Fig. 5. THG signal ratio S_{2200}/S_{1700} as a function of imaging depth z. The ratio is normalized such that $S_{2200}/S_{1700} = 1$ at $z = 160\,\mu$m.

Table 1. The measured SBR at different depths.

Depths (μm)	1700 nm	2200 nm
160	3968	8598
190	2071	3525
220	1021	1838
250	677	899

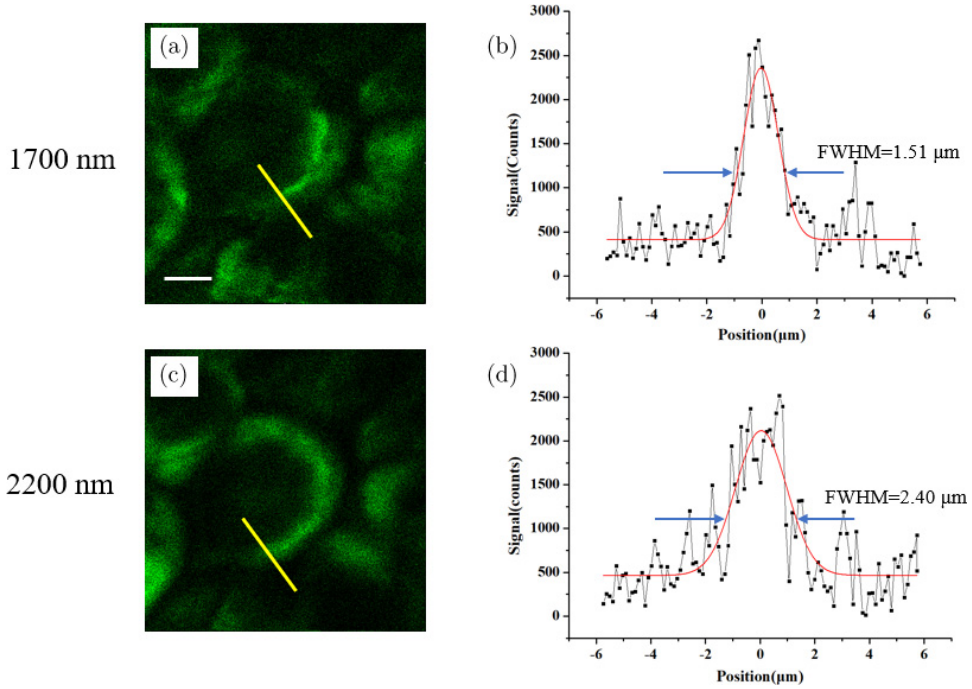

Fig. 6. (Color online) THG image of adipocytes 170 μm below the skin surface, excited at 1700 nm (a) and 2200 nm (c). The measured line profiles (black squares) along the yellow lines in (a) and (c) are shown in (b) and (d), respectively. The Gaussian fits (red curves) with measured FWHMs and are also indicated in (b) and (d). Scale bars: 10 μm.

Table 2. The measured FWHMs in the adipocyte membrane.

Position	1700 nm (μm)	2200 nm (μm)
1	1.74	2.49
2	1.51	2.40
3	1.23	2.33
Mean	1.49	2.40

fitting, yielding FWHM values for both excitations. This whole procedure was repeated three times along different positions of the adipocyte. The measured FWHMs following this procedure are listed in Table 2. The mean FWHMs are 1.49 μm for 1700 nm and 2.40 μm for 2200 nm excitation, respectively. This lower spatial resolution of the 2200 nm THG imaging is due to its longer wavelength.

4. Discussion

If we compare the *ex vivo* transmittance measurement and *in vivo* imaging results, we can readily see the discrepancy: *Ex vivo* measurement shows that higher transmittance favors the 1700 nm window, rather than the 2200 nm window; however, *in vivo* THG imaging shows the opposite: with the same optical power on the skin surface, 2200 nm excitation images are deeper. We think this discrepancy may be due to the following: (1) *Ex vivo* biological sample is by no means is the same as *in vivo* sample. One example is that for deep-brain imaging in mouse, once the mouse dies, the imaging depth quickly drops given all other conditions are the same. This indicates that the nature of biological tissues may have changed before and after death. In order to test this hypothesis, we performed comparative THG imaging on mouse skin *in vivo* first, then we sacrificed the mouse and performed in the same area (which was essentially *ex vivo* imaging). The calculated signal ratio S_{2200}/S_{1700} in Fig. 5, based on imaging, shows a similar behavior as imaging depth increases. This proves the vitality of the mouse cannot explain the deeper penetration of 2200 nm. (2) So far, we have only compared excitation wavelengths. THG signals are also different: 567 nm for 1700 nm and 733 nm for 2200 nm, respectively. According to *ex vivo* measurement, transmittance at 733 nm is higher than that at 567 nm. For simplicity, if we assume that the skin is homogeneous, the effective attenuation length (l_e) is calculated to be 0.0957 mm for 733 nm and 0.0849 mm for 567 nm, respectively. If we assume

that THG signals also decay exponentially in the skin, the normalized THG signal ratio $\frac{S_{733\,\mathrm{nm}}}{S_{567nm}} = e^{-z/l_e(733\,\mathrm{nm})}/e^{-z/l_e(567\,\mathrm{nm})}$ will increase as imaging depth increases, partly explaining the deeper penetration of 2200 nm THG imaging. We note that this emission wavelength explanation is similar to that in brain MPM.[23] (3) Depth-dependent aberration is different between the two excitation wavelengths. Aberration is the accumulated phase from surface to the focus, and is inversely proportional to wavelength. Theoretically, after traversing the same tissue, longer wavelength accumulates less aberration than shorter excitation wavelength. It is well-known that the larger the aberration is, the poorer the multiphoton signal is. For example, in Ref. 24, we have shown that spherical aberration induced multiphoton signal degradation decreases as the excitation wavelength shifts from 850 nm to 1300 nm and 1700 nm. Using the same theoretical model, we also calculated spherical aberration-induced multiphoton signal degradation at 2200 nm and compared it to 1700 nm. Our results in Fig. 7 indicate that as imaging depth increases, 1700 nm suffers more from spherical aberration-induced multiphoton signal degradation compared with 2200 nm. So, both emission wavelength difference and aberration may be the contributing factors for the deeper penetration of 2200 nm excitation into the skin, compared to that of the 1700 nm excitation.

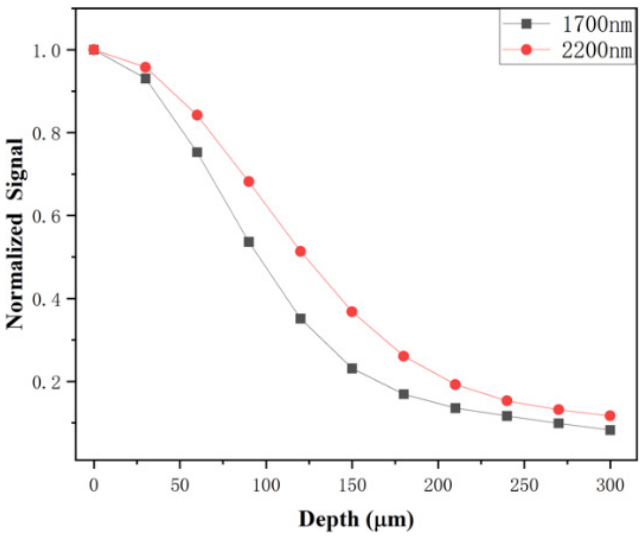

Fig. 7. Spherical aberration-induced multiphoton signal degradation decreases as the depths increase, excited at 1700 and 2200 nm.

5. Conclusions

In the previous work, we demonstrated the deep-brain imaging capability at the 2200 nm window, but as for the imaging effectiveness or spatial resolution of 3 PM, 1700 nm window performed better.[19] As is known to all, the skin is a multilayered structure, and thus, highly heterogenous imposing scattering and aberration onto the excitation light. Intuitively, low scattering and low aberration at 2200 nm is more advantageous. In this paper, *ex vivo* broadband transmittance measurement clearly shows that the skin has a local maximum transmittance at this window. Furthermore, our *in vivo* THG imaging shows that with 9 mW optical power on the skin surface, structures of 220 μm below the skin surface can be resolved, and THG signals can still be generated at a depth of 250 μm. So far, the maximum imaging depth is limited by the available optical power on the sample. We expect that this imaging depth can be further extended, given that higher optical power on the sample can be achieved by optimizing both the laser source and the overall transmittance of the imaging system. We also note that with 9 mW optical power on the skin surface, we did not observe any structural damage to the skin.

Acknowledgments

This work was supported by National Natural Science Foundation of China (NSFC) (Nos. 61775143, 61975126 and 62075135); the Science and Technology Innovation Commission of Shenzhen under Nos. JCYJ20190808174819083, JCYJ20190808175201640 and KQTD20150710165601017; and China Postdoctoral Science Foundation (No. 2021M702241). Xinlin Chen and Yi Pan contributed equally to this work.

Conflicts of Interest

The authors declare that there are no conflicts of interest relevant to this article.

References

1. W. Denk, J. H. Strickler, W. W. Webb, "Two-photon laser scanning fluorescence microscopy," *Science* **248**(4951), 73–76 (1990).

2. F. Helmchen, W. Denk, "Deep tissue two-photon microscopy," *Nat. Methods* **2**(12), 932–940 (2005).
3. W. R. Zipfel, R. Williams, W. W. Webb, "Live tissue intrinsic emission microscopy using multiphoton-excited native fluorescence and second harmonic generation," *Proc. Natl. Acad. Sci. USA* **100**(12), 7075–7080 (2003).
4. C. Dong, B. Yu, P. D. Kaplan, P. T. C. So, "Performances of high numerical aperture water and oil immersion objective in deep-tissue, multi-photon microscopic imaging of excised human skin," *Microsc. Res. Technol.* **63**(1), 81–86 (2010).
5. L. H. Laiho, S. Pelet, T. M. Hancewicz, P. D. Kaplan, P. T. C. So, "Two-photon 3-D mapping of *ex vivo* human skin endogenous fluorescence species based on fluorescence emission spectra," *J. Biomed. Opt.* **10**(2), 24016 (2005).
6. M. J. Koehler, A. Preller, N. Kindler, P. Elsner, M. Kaatz, "Intrinsic, solar and sunbed-induced skin aging measured *in vivo* by multiphoton laser tomography and biophysical methods," *Skin Res. Technol.* **15**(3), 357–363 (2010).
7. C. Szu-Yu, C. Shee-Uan, W. Hai-Yin, L. Wen-Jeng, L. Yi-Hua, S. Chi-Kuang, "*In Vivo* virtual biopsy of human skin by using noninvasive higher harmonic generation microscopy," *IEEE J. Sel. Top. Quantum Electron.* **16**(3), 478–492 (2010).
8. E. Chaigneau, A. J. Wright, S. P. Poland, J. M. Girkin, R. A. Silver, "Impact of wavefront distortion and scattering on 2-photon microscopy in mammalian brain tissue," *Opt. Express* **19**(23), 22755–22774 (2011).
9. J. Zeng, P. Mahou, M. C. Schanne-Klein, E. Beaurepaire, D. Débarre, "3D resolved mapping of optical aberrations in thick tissues," *Biomed. Opt. Express* **3**(8), 1898–1913 (2012).
10. N. G. Horton, K. Wang, D. Kobat, C. G. Clark, F. W. Wise, C. B. Schaffer, C. Xu, "*In vivo* three-photon microscopy of subcortical structures within an intact mouse brain," *Nat. Photonics* **7**(3), 205–209 (2013).
11. M. Wang, C. Wu, D. Sinefeld, B. Li, F. Xia, C. Xu, "Comparing the effective attenuation lengths for long wavelength *in vivo* imaging of the mouse brain," *Biomed. Opt. Express* **9**(8), 3534–3543 (2018).
12. P. Qiu, C. He, "Degradation of multiphoton signal and resolution when focusing through a planar interface with index mismatch: Analytical approximation and numerical investigation," *J. Innov. Opt. Health Sci.* **11**(4), 1850020 (2018).
13. C. He, X. Deng, Y. Pan, S. Tong, J. Kang, J. Li, P. Qiu, K. Wang, "3-photon microscopy of myelin in mouse digital skin excited at the 1700-nm window," *J. Biophotonics* **13**(12), e202000321 (2020).
14. C. He, M. Gan, X. Deng, H. Liu, P. Qiu, K. Wang, "3-photon fluorescence imaging of sulforhodamine B-labeled elastic fibers in the mouse skin *in vivo*," *J. Biophotonics* **12**(11), e201900185 (2019).
15. K. Wang, Y. Pan, S. Tong, H. Liang, P. Qiu, "Deep-skin multiphoton microscopy of lymphatic vessels excited at the 1700-nm window *in vivo*," *Biomed. Opt. Express* **12**(10), 6474–6484 (2021).
16. Y. Wang, W. Wen, K. Wang, P. Zhai, P. Qiu, K. Wang, "Measurement of absorption spectrum of deuterium oxide (D_2O) and its application to signal enhancement in multiphoton microscopy at the 1700-nm window," *Appl. Phys. Lett.* **108**(2), 21112 (2016).
17. L. Shi, L. A. Sordillo, A. Rodriguez-Contreras, R. Alfano, "Transmission in near-infrared optical windows for deep brain imaging," *J. Biophotonics* **9**(1–2), 38–43 (2016).
18. S. Golovynskyi, I. Golovynska, L. I. Stepanova, O. I. Datsenko, L. Liu, J. Qu, T. Y. Ohulchanskyy, "Optical windows for head tissues in near-infrared and short-wave infrared regions: Approaching transcranial light applications," *J. Biophotonics* **11**(12), e201800141 (2018).
19. X. Chen, S. Tong, W. Zhang, X. Deng, H. Cheng, Y. Pan, W. Xie, P. Qiu, K. Wang, "*In vivo* three-photon microscopy of mouse brain excited at the 2200 nm window," *ACS Photonics* **8**(10), 2898–2903 (2021).
20. F. M. Mitschke, L. F. Mollenauer, "Discovery of the soliton self-frequency shift," *Opt. Lett.* **11**(10), 659–661 (1986).
21. K. Wang, N. G. Horton, K. Charan, C. Xu, "Advanced fiber soliton sources for nonlinear deep tissue imaging in biophotonics," *IEEE J. Sel. Top. Quantum Electron.* **20**(2), 50–60 (2014).
22. K. Wang, W. Wen, H. Liu, Y. Du, Z. Zhuang, P. Qiu, "Transmittance characterization of objective lenses covering all four near infrared optical windows and its application to three-photon microscopy excited at 1820 nm," *IEEE Photonics J.* **10**(3), 1–7 (2018).
23. M. Wang, M. Kim, F. Xia, C. Xu, "Impact of the emission wavelengths on *in vivo* multiphoton imaging of mouse brains," *Biomed. Opt. Express* **10**(4), 1905–1918 (2019).